

Tensions with the flat Λ CDM model from high-redshift cosmography

G. Bargiacchi,^{1,2*} M. G. Dainotti,^{3,4,5} S. Capozziello^{1,2,6}

¹*Scuola Superiore Meridionale, Largo S. Marcellino 10, 80138 Napoli, Italy*

²*Istituto Nazionale di Fisica Nucleare (INFN), Sez. di Napoli, Complesso Univ. Monte S. Angelo, Via Cinthia 9, 80126, Napoli, Italy*

³*National Astronomical Observatory of Japan, 2 Chome-21-1 Osawa, Mitaka, Tokyo 181-8588, Japan*

⁴*The Graduate University for Advanced Studies, SOKENDAI, Shonankokusaimura, Hayama, Miura District, Kanagawa 240-0193, Japan*

⁵*Space Science Institute, 4765 Walnut St, Suite B, 80301 Boulder, CO, USA*

⁶*Dipartimento di Fisica "E. Pancini", Università degli Studi di Napoli Federico II, Complesso Univ. Monte S. Angelo, Via Cinthia 9, 80126, Napoli, Italy*

Accepted XXX. Received YYY; in original form ZZZ

ABSTRACT

The longstanding search for the cosmological model that best describes the Universe has been made more intriguing since the recent discovery of the Hubble constant, H_0 , tension observed between the value of H_0 from the Cosmic Microwave Background and from type Ia supernovae (SNe Ia). Hence, the commonly trusted flat Λ CDM model is under investigation. In this scenario, cosmography is a very powerful technique to investigate the evolution of the Universe without any cosmological assumption, thus revealing tensions between observational data and predictions from cosmological models in a completely model-independent way. We here employ a robust cosmographic technique based on an orthogonal logarithmic polynomial expansion of the luminosity distance to fit quasars (QSOs) alone and QSOs combined with Gamma-Ray Bursts (GRBs), SNe Ia, and Baryon Acoustic Oscillations. To apply QSOs and GRBs as probes we use, respectively, the Risaliti-Lusso relation between ultraviolet and X-ray luminosities and the “Dainotti GRB 3D relation” among the rest-frame end time of the X-ray plateau emission, its corresponding luminosity, and the peak prompt luminosity. We also correct QSOs and GRBs for selection biases and redshift evolution and we employ both the traditional Gaussian likelihood and the newly discovered best-fit likelihoods for each probe investigated. This comprehensive analysis reveals a strong tension ($> 4\sigma$) between our data sets and the flat Λ CDM model proving the power of both the cosmographic approach and high-redshift sources, such as QSOs and GRBs, which can probe the Universe at early epochs.

Key words: cosmology: theory - methods: analytical - cosmological parameters

1 INTRODUCTION

Cosmological probes such as type Ia supernovae (SNe Ia; Riess et al. 1998; Perlmutter et al. 1999) and the combination of SNe Ia, Baryonic Acoustic Oscillations (BAOs), Cosmic Microwave Background (CMB), and lensing (Planck Collaboration et al. 2020) have proved that the Universe is currently in a phase of accelerated expansion, which is commonly ascribed to a dark energy component. According to the Λ cold dark matter (CDM) model (Λ CDM), this dark energy component is a cosmological constant (Λ) originated by vacuum quantum fluctuations (Sahni & Starobinsky 2000; Carroll 2001; Peebles & Ratra 2003). Nevertheless, the discrepancy between the current theoretical and observed value of Λ poses the cosmological constant problem (Weinberg 1989). This problem historically questions the Λ CDM model, together with other well-known theoretical issues, such as the fine-tuning and the coincidence problems. On the other hand, the flat Λ CDM model can well reproduce several observations from SNe Ia, BAOs, and CMB. This interesting puzzle regarding the flat Λ CDM model has been recently made more intriguing by the discovery of the Hubble constant, H_0 , tension. Indeed, the H_0 value inferred from the CMB, assuming a flat Λ CDM

model ($H_0 = 67.4 \pm 0.5 \text{ km s}^{-1} \text{ Mpc}^{-1}$, Planck Collaboration et al. 2020), is incompatible, at $\geq 4\sigma$ with the value measured locally from Cepheids and SNe Ia ($H_0 = 73.04 \pm 1.04 \text{ km s}^{-1} \text{ Mpc}^{-1}$, Riess et al. 2022), and with that reported in Wong et al. (2020) obtained from lensed quasars ($H_0 = 73.3 \pm 1.7 \text{ km s}^{-1} \text{ Mpc}^{-1}$). Other cosmological probes have been further employed to shed light on this tension showing even a more complex scenario. For example, cosmic chronometers tend to a H_0 value close to the one of the CMB (Gómez-Valent & Amendola 2018), while time-delay and strong lensing of quasars (QSOs) prefer the one of SNe Ia (Liao et al. 2019), and other probes, such as QSOs (Lenart et al. 2023), the Tip of the Red-Giant Branch (TRGB; Freedman 2021), and Gamma-Ray Bursts (GRBs; Cardone et al. 2009; Dainotti et al. 2013a; Postnikov et al. 2014; Dainotti et al. 2021c, 2022c,a,e) show a H_0 value halfway between the one of SNe Ia and the one of CMB. Many theoretical works have been discussed to explain this tension (Di Valentino et al. 2021; Dainotti et al. 2021c; Schiavone et al. 2022).

In this framework, techniques which are completely independent from the cosmology are among the most powerful tools that have been so far proposed to unveil the actual structure of the Universe without any cosmological assumption. In this regard, cosmography (Weinberg 1972) is one of the most consolidated approaches. It relies only on the isotropy and homogeneity of the Universe by assuming the

* Corresponding author, E-mail: giada.bargiacchi@unina.it

Friedmann-Lemaître-Robertson-Walker (FLRW) metric. As a consequence, cosmography provides a description of the Universe which is purely geometrical and where all the physics is embedded in the scale factor $a(t)$ of the FLRW metric. Nevertheless, it does not need an explicit expression for $a(t)$, but only an analytical form for it. Hence, this technique supplies a completely model-independent way to investigate the evolution of the Universe. The main advantage of this approach is that, if the investigated cosmographic parameterization has a number of free parameters that makes it sufficiently flexible, it can fit the data with high accuracy, and then the obtained cosmographic parameters can be used to test any cosmological model (Capozziello et al. 2018; Escamilla-Rivera & Capozziello 2019). More precisely, if we expand the considered cosmological model and the cosmographic expansion, we obtain the relations between the free cosmological and cosmographic parameters (Aviles et al. 2014; Capozziello et al. 2019; Benetti & Capozziello 2019), see also Section 3.4. These relations allow us to compare the best-fit of the cosmographic model with the prediction of the investigated cosmological model (see e.g. Riess et al. 2004). Nonetheless, the cosmographic approach presents one major issue: as in cosmological studies, high-redshift (i.e. $z > 2$) sources are essential to investigate possible deviations from the theoretical predictions of cosmological models, but in the high-redshift interval convergence issues may emerge in the cosmographic expansion (see e.g. Capozziello et al. 2020). The traditional Taylor expansion commonly used in cosmography to analytically approximate $a(t)$ (Visser 2004; Capozziello et al. 2019) is an example of this problem. Indeed, following the definition of the Taylor expansion, it gives an approximate expression of the luminosity distance $D_L(z)$ around $z = 0$, and thus can be applied only in the limit $z \leq 1$ and not to high-redshift probes, such as QSOs and GRBs, observed up to $z = 7.64$ (Wang et al. 2021) and $z = 9.4$ (Cucchiara et al. 2011), respectively. Moreover, also SNe Ia have been recently observed up to $z = 2.26$ (Rodney et al. 2015) by the *Pantheon* survey (Scolnic et al. 2018), which marks the problem of applying the Taylor expansion in cosmography.

While SNe Ia are commonly trusted as the most reliable and powerful standard candles in cosmology, QSOs and GRBs have only been recently promoted to cosmological tools, attracting more and more the interest of the cosmological community due to their invaluable role at high redshifts. To employ QSOs as cosmological probes, we use the X-ray to ultraviolet (UV) relation (X-UV relation), also called Risali-Lusso relation (RL), between the UV and X-ray luminosities. This correlation was proposed after the first X-ray surveys (Tananbaum et al. 1979; Zamorani et al. 1981; Avni & Tananbaum 1986), and then validated with different QSO samples (e.g. Steffen et al. 2006; Just et al. 2007; Lusso et al. 2010; Lusso & Risaliti 2016; Bisogni et al. 2021). This relation is physically supported by the commonly accepted theoretical model in which the emission of QSOs is supplied by the accretion on a central supermassive black hole, which converts mass into energy with high efficiency (Srianand & Gopal-Krishna 1998; Horowitz & Teukolsky 1999; Netzer 2013; Kroupa et al. 2020). The RL relation has been successfully employed for cosmological applications (Risaliti & Lusso 2015, 2019; Lusso et al. 2020; Bargiacchi et al. 2021, 2022; Dainotti et al. 2022h; Khadka & Ratra 2020a,b, 2021; Colgáin et al. 2022b; Khadka & Ratra 2022; Colgáin et al. 2022a; Wang et al. 2022; Li et al. 2022; Lenart et al. 2023; Bargiacchi et al. 2023; Dainotti et al. 2023c; Dainotti et al. 2023a). The reliability of this relation for cosmological purposes has also been recently proved by Dainotti et al. (2022h), which have accounted for selection biases and redshift evolution of QSO luminosities. Analogously, GRBs can be standardized as cosmological tools through the GRB fundamental plane relation, also named the

three-dimensional (3D) Dainotti relation, which is an implementation of the previous two-dimensional relation, among the rest-frame time at the end of the plateau emission, T_{χ}^* , the corresponding X-ray luminosity of the light curve, L_{χ} (Dainotti et al. 2008, 2010, 2011, 2017a), and the prompt peak luminosity, L_{peak} (Dainotti et al. 2016, 2017b, 2020a; Srinivasaragavan et al. 2020). This relation is theoretically supported by the magnetar model (Zhang & Mészáros 2001; Dall’Osso et al. 2011; Bernardini et al. 2012; Rowlinson et al. 2014; Rea et al. 2015). The two-dimensional Dainotti relation and the fundamental plane relation have already been applied in several cosmological studies (Cardone et al. 2009, 2010; Postnikov et al. 2014; Dainotti et al. 2013a, 2022b,g,a; Bargiacchi et al. 2023; Dainotti et al. 2023c). The two-dimensional Dainotti relation has also been discovered in optical (Dainotti et al. 2020c, 2022i) and radio (Levine et al. 2022), while the 3D correlation has also been found in high energy γ -rays (Dainotti et al. 2021b) and in optical (Dainotti et al. 2022f). For a more extensive discussion on the GRB correlations see also Dainotti & Del Vecchio (2017), Dainotti & Amati (2018), and Dainotti et al. (2018).

The combination of traditional low-redshift cosmological probes, such as SNe Ia and BAOs, and promising high-redshift sources, such as QSOs and GRBs, allows us to effectively unveil tensions between the observations and the standard cosmological model through the cosmographic approach (see e.g. Rezaei et al. 2020). However, this is possible only if the above-described convergence issues are solved. To this end, some techniques have been proposed, as for example rational polynomials such as the Padé and Chebyshev polynomials (see e.g. Aviles et al. 2014; Capozziello et al. 2018; Demianski et al. 2017; Zamora Munõz & Escamilla-Rivera 2020). In this paper, we make use of a cosmographic technique based on the expansion of the luminosity distance in orthogonal polynomials of logarithmic functions. The robustness and reliability of this approach has already been discussed in detail and proved in Bargiacchi et al. (2021). This cosmographic model, indeed, completely overcomes the weakness of the Taylor expansion at high redshifts providing a suitable analytical reproduction of observational data and cosmological models to test physical models. We stress that here the cosmographic approach is applied starting from QSOs as the major cosmological player.

We here leverage the power of this cosmographic technique to separately fit QSOs alone and QSOs joint with GRBs, SNe Ia from the *Pantheon* + release, and BAOs to test the flat Λ CDM model. This allows us to unveil and quantify tensions between this cosmological model and the considered observational data through a completely model-independent technique. We also compare different treatments for the correction for redshift evolution of luminosities of QSOs and GRBs, and different likelihoods to show to what extent these choices affect the results. Compared to previous cosmographic analyses in which QSOs have been employed, this work manifestly presents several points of novelty. It is indeed the first time in the cosmographic realm that the most updated sample of QSOs is used in the whole redshift range of observations, including also low-redshift sources, as standalone probe and also combined with the latest samples of GRBs and SNe Ia. Moreover, the correction for selection biases and redshift evolution and the application of likelihoods different from the Gaussian one, which are crucial to properly and better estimate the parameters, have never been implemented in cosmography before.

The manuscript is structured as follows. Section 2 describes the samples of QSOs, GRBs, SNe Ia, and BAO. Section 3 introduces the cosmographic model, how it can be compared to the predictions of the flat Λ CDM model, the physical quantities investigated for each probe, the technique applied to account for selection biases and correct for redshift evolution, and the fitting procedure with different

likelihoods. In Section 4, we outline our results, also compared with previous works. Finally, in Section 5 we summarize our conclusions.

2 DATA SETS

In this work, we use both QSOs alone and QSOs combined with GRBs, SNe Ia from the *Pantheon+* sample, and BAOs. The QSO data set is the one composed of 2421 sources described in detail in Lusso et al. (2020). This sample has been built combining eight different sub-samples present in archives and in the literature and is the most updated QSO catalog specifically released for cosmological purposes. Indeed, these sources have been carefully selected based on several criteria both in X-ray and UV bands (e.g. signal-to-noise ratio, the host galaxy contamination in UV, the absorption in X-ray, the Eddington bias) to remove as many as possible observational biases (see Lusso et al. 2020, for details). Despite Lusso et al. (2020), as in other recent works (Dainotti et al. 2022h; Lenart et al. 2023; Bargiacchi et al. 2023; Dainotti et al. 2023c; Dainotti et al. 2023a), we here employ all the 2421 sources which cover the redshift range $z = 0.009 - 7.54$ to avoid imposing an arbitrary truncation in the redshift distribution of the sources and to leverage also the power of low-redshift QSOs to constrain parameters.

As GRB data set, we employ the ‘‘Platinum’’ sample (Dainotti et al. 2020b), which has been further improved compared to the previous golden sample (Dainotti et al. 2016, 2017b, 2020b). It consists of 50 X-ray observations ranging from $z = 0.055$ to $z = 5$ which verify the following requirements: a) the plateau must have an inclination $< 41^\circ$, b) it must present at least 5 points in its beginning to allow a determination of the onset, c) it must not show flares, d) and it must last > 500 s (see also Dainotti et al. 2022a,g). This selection leads to the Platinum sample of 50 sources starting from 222 GRBs with a known redshift observed from January 2005 to August 2019 by the *Neil Gehrels Swift Observatory* (Swift). These data are taken from the Swift Burst Analyser (Evans et al. 2009), which includes (BAT), X-Ray Telescope (XRT), and optical (UVOT) repositories. These GRBs possess a plateau that can be fitted applying the Willingale et al. (2007) model.

For SNe Ia, we use the most up-to-date sample from the *Pantheon+* release (Scolnic et al. 2022), which has improved the previous *Pantheon* sample (Scolnic et al. 2018) with additional low-redshift observations. It is indeed composed of 1701 sources (compared to the 1048 of the *Pantheon* data set) gathered from 18 surveys in the redshift range between $z = 0.001$ and $z = 2.26$.

The BAO data set here considered is the one of 26 points between $z = 0.106$ (Beutler et al. 2011) and $z = 2.36$ (Font-Ribera et al. 2014) described in Sharov & Vasiliev (2018) with the covariance matrix provided by Sharov (2016). This is the same collection already employed in Dainotti et al. (2022d), Dainotti et al. (2022b), Dainotti et al. (2022a), Bargiacchi et al. (2023), and Dainotti et al. (2023c).

3 METHODS

3.1 The physical quantities

We here define the physical quantities we investigate for each probe separately to perform the fit of our cosmographic model. More precisely, we consider the distance moduli for SNe Ia and GRBs, the luminosities for QSOs, and the distance measure for BAOs. These choices have already been described in detail and justified in Dainotti et al. (2022g), Dainotti et al. (2022a), Bargiacchi et al. (2023) and Dainotti et al. (2023c).

To standardize QSOs as cosmological probes, we use the X-UV relation

$$\log_{10} L_X = g_1 \log_{10} L_{UV} + n_1 \quad (1)$$

where L_X and L_{UV} are the luminosities (in $\text{erg s}^{-1} \text{Hz}^{-1}$) at 2 keV and 2500 Å, respectively. These luminosities are computed from the observed flux densities F_X and F_{UV} (in $\text{erg s}^{-1} \text{cm}^{-2} \text{Hz}^{-1}$), respectively, using $L_{X,UV} = 4\pi D_L^2 F_{X,UV}$. Indeed the K-correction (Bloom et al. 2001) is omitted for QSOs since their spectral index γ_Q is assumed to be 1 in $K = (1+z)^{\gamma_Q-1}$, leading to $K = 1$ (Lusso et al. 2020). In addition, we also need to correct L_X and L_{UV} for evolutionary effects and selection biases, as detailed in Sect. 3.2 and as already shown in Dainotti et al. (2013b), Dainotti et al. (2015), Dainotti et al. (2022h), Lenart et al. (2023), Bargiacchi et al. (2023), Dainotti et al. (2023c), and Dainotti et al. (2023a). The parameters g_1 and n_1 , and the intrinsic dispersion sv_1 of the RL relation, can be fitted through the Kelly technique (Kelly 2007), which is a Bayesian method based on the Markov Chain Monte Carlo (MCMC) approach that allows us to account for uncertainties on all quantities and also for the intrinsic dispersion of the relation. Using $\log_{10} L_{UV} = \log_{10}(4\pi D_L^2) + \log_{10} F_{UV}$ in Eq. (1), we obtain the observed physical quantity $\log_{10} L_{X,obs}$ under the assumption of the RL relation:

$$\log_{10} L_{X,obs} = g_1 \left[\log_{10}(4\pi D_L^2) + \log_{10} F_{UV} \right] + n_1. \quad (2)$$

The theoretical quantity is derived as $\log_{10} L_{X,th} = \log_{10}(4\pi D_L^2) + \log_{10} F_X$. In both $\log_{10} L_{X,obs}$ and $\log_{10} L_{X,th}$, the luminosity distance D_L (in Megaparsec, Mpc) is given by Eq. (9) and thus depends on the cosmographic parameters, the redshift, and H_0 .

To employ GRBs as cosmological probes, we apply the 3D X-ray fundamental plane relation which reads as:

$$\log_{10} L_X = a \log_{10} T_X^* + b \log_{10} L_{peak} + c_1 \quad (3)$$

where the luminosities L are obtained from the measured fluxes F through the relation $L = 4\pi D_L^2 \cdot F \cdot K$, where D_L is expressed in units of cm and K is the K-correction. In the case of GRBs, since their spectrum can be reproduced with a simple power-law, this correction can be written in terms of the spectral index of the X-ray plateau, γ , as $K = (1+z)^{\gamma-1}$. As for QSOs, the free parameters a , b , and c_1 can be evaluated by fitting the 3D relation with the Kelly technique along with the intrinsic dispersion sv of the relation. The quantities L_X , T_X^* , and L_{peak} in Eq. (3) should also be corrected for their redshift evolution (Dainotti et al. 2022a; Bargiacchi et al. 2023; Dainotti et al. 2023c), as detailed in Sect. 3.2. Assuming the 3D relation, we can derive (Dainotti et al. 2022a) the observed μ for GRBs, $\mu_{obs,GRBs}$, which represents the physical quantity of our interest. Indeed, using the above-defined relation between luminosities and fluxes to convert luminosities into fluxes in Eq. (3) and imposing $\mu = 5 \log_{10} D_L + 25$, we obtain

$$\mu_{obs,GRBs} = 5 \left[-\frac{\log_{10} F_X}{2(1-b)} + \frac{b \cdot \log_{10} F_{peak}}{2(1-b)} - \frac{(1-b) \log_{10}(4\pi) + c_1}{2(1-b)} + \frac{a \log_{10} T_X^*}{2(1-b)} \right] + 25 \quad (4)$$

where the K-correction has already been applied to all quantities. In this equation, we fix $c_1 = 23$, as derived in Dainotti et al. (2022a). The theoretical μ is defined as

$$\mu_{th} = 5 \log_{10} D_L + 25 \quad (5)$$

where D_L is given by Eq. (9).

For SNe Ia, we use the distance modulus μ defined as $\mu = m - M$,

with m and M the apparent and absolute magnitude, respectively. Since M is degenerate with H_0 , we cannot determine H_0 by using SNe Ia alone (Tripp 1998; Scolnic et al. 2018), but H_0 can be derived by fixing M . In this regard, we directly apply the distance moduli observed, $\mu_{obs, SNe Ia}$, reported by the *Pantheon+* release¹, which are computed by fixing M to $M = -19.253 \pm 0.027$, as obtained in Riess et al. (2022) considering 42 SNe Ia combined with Cepheids hosted in the same galaxies of these SNe Ia. Due to their degeneracy, this assumption on M implies $H_0 = 73.04 \pm 1.04 \text{ km s}^{-1} \text{ Mpc}^{-1}$ Riess et al. (2022). The theoretical μ is the same defined in Eq. (5).

Regarding BAOs, the considered physical quantity is $d_z = r_s(z_d)/D_V(z)$ (e.g. Eisenstein et al. 2005), where $r_s(z_d)$ is the sound horizon at the baryon drag epoch z_d and $D_V(z)$ is the volume averaged distance. We use the observed $d_{z,obs}$ of Sharov & Vasiliev (2018) which are computed from the measured $D_V(z)$ by assuming the fiducial value $(r_s(z_d) \cdot h)_{fid} = 104.57 \text{ Mpc}$, where h is the dimensionless Hubble constant $h = H_0/100 \text{ km s}^{-1} \text{ Mpc}^{-1}$ (see Sharov 2016). To estimate the theoretical $d_{z,th}$ we use the following numerical approximation (Aubourg et al. 2015; Cuceu et al. 2019), since the exact calculation for $r_s(z_d)$ would require the application of Boltzmann codes:

$$r_s(z_d) \sim \frac{55.154 e^{-72.3(\Omega_b h^2 + 0.0006)^2}}{(\Omega_M h^2)^{0.25351} (\Omega_b h^2)^{0.12807}} \text{ Mpc} \quad (6)$$

where Ω_M , Ω_b and Ω_ν are the current matter, baryon and neutrino density parameters. In this formula, we fix $\Omega_\nu h^2 = 0.00064$ and $\Omega_b h^2 = 0.002237$ according to Hinshaw et al. (2013) and Planck Collaboration et al. (2020)). The theoretical distance $D_V(z)$ required to compute $d_{z,th}$ is defined as Eisenstein et al. (2005)

$$D_V(z) = \left[\frac{cz}{H(z)} \frac{D_L^2(z)}{(1+z)^2} \right]^{\frac{1}{3}}. \quad (7)$$

3.2 Treatment of redshift evolution and selection biases

Since GRBs and QSOs are observed up to high-redshifts, we need to correct their observed quantities for possible selection biases and evolutionary effects, which could distort or induce a correlation between physical quantities, thus inducing an incorrect determination of parameters (Dainotti et al. 2013a). To apply these corrections, we employ the Efron & Petrosian (EP) statistical method (Efron & Petrosian 1992) already used in several works for GRBs (Dainotti et al. 2013a, 2015, 2017a, 2021a, 2022a; Bargiacchi et al. 2023; Dainotti et al. 2023c) and in the QSO realm (Dainotti et al. 2022h; Lenart et al. 2023; Bargiacchi et al. 2023; Dainotti et al. 2023c; Dainotti et al. 2023a). In our study, we use the results of Dainotti et al. (2023c) for the platinum sample of GRBs and Dainotti et al. (2022h) for QSOs and we here just summarize their procedure and outcomes.

In this method, the investigated physical quantities (i.e. luminosities and time) are assumed to evolve with z according to $L' = \frac{L}{(1+z)^k}$ and $T' = \frac{T}{(1+z)^k}$, where L and T are the observed quantities, L' and T' the corresponding corrected ones without evolution, and k the parameter that mimics the evolution. Nonetheless, the choice of the functional form as a power-law does not affect the results (Singal et al. 2011; Dainotti et al. 2021d, 2022h) and hence we could also parameterize the dependence on the redshift through more complex functions. Then, the Kendall's τ statistic is applied to identify

the k value that eliminates the evolution with the redshift. In this procedure, τ is defined as

$$\tau = \frac{\sum_i (\mathcal{R}_i - \mathcal{E}_i)}{\sqrt{\sum_i \mathcal{V}_i}}. \quad (8)$$

where i flows along the sources that at z_i present a luminosity greater than the minimum observable luminosity ($L_{min,i}$) at that redshift. $L_{min,i}$ is computed by requiring a limiting flux. The value of this flux threshold is chosen such that the retained sample is composed at least of 90% of the total initial sources and that it resembles the overall original distribution according to the Kolmogorov-Smirnov test (Dainotti et al. 2013a, 2015, 2017a; Levine et al. 2022; Dainotti et al. 2022h,g). \mathcal{R}_i is the rank defined as the number of points in the associated set of the i -source, where the associated set consists of all j -points for which $z_j \leq z_i$ and $L_{z_j} \geq L_{min,i}$. \mathcal{R}_i is thus computed for each point by considering the position of the source in the sample and including all the sources that can be detected for particular observational limits. In this way the Kendall's statistics is able to take into account and correct for the presence of selection biases in the data, such as the flux limit and temporal resolution of the instrument (see e.g. Efron & Petrosian 1992; Kocevski & Liang 2006; Petrosian et al. 2009; Dainotti et al. 2013a,b, 2022h, for further details). In Eq. (8), $\mathcal{E}_i = \frac{1}{2}(i+1)$ and $\mathcal{V}_i = \frac{1}{12}(i^2+1)$ are the expectation value and variance, respectively, when the evolution with redshift has been removed. As a consequence, the correlation with redshift disappears when $\tau = 0$, which allows us to obtain the value of k that removes the dependence. The condition $|\tau| > n$ implies that the hypothesis of uncorrelation is rejected at $n\sigma$ level, hence it provides us with the 1σ uncertainty on the k value by imposing $|\tau| \leq 1$. The found value of k can now be used to determine L' (and straightforwardly T' by replacing the luminosity with the time in this procedure) for the total sample. The k values derived through this procedure for luminosities and time that we here apply are: $k_{L_{peak}} = 1.37^{+0.83}_{-0.93}$, $k_{T_\gamma} = -0.68^{+0.54}_{-0.82}$, and $k_{L_\gamma} = 0.44^{+1.37}_{-1.76}$ for GRBs (Dainotti et al. 2023c), and $k_{UV} = 4.36 \pm 0.08$ and $k_X = 3.36 \pm 0.07$ for QSOs (Dainotti et al. 2022h). The de-evolved quantities computed with these k values are the ones used in our fits when accounting for the redshift evolution.

Nevertheless, from the description of the EP method, is clear that k is obtained assuming a specific cosmological model, needed to compute the luminosities from the fluxes. We refer to this approach, in which the evolution is taken into account but assuming a specific cosmological model, as "fixed" correction. In both the works we are referring to (i.e. Dainotti et al. 2022h, 2023c), the assumed model is a flat Λ CDM model with $\Omega_M = 0.3$ and $H_0 = 70 \text{ km s}^{-1} \text{ Mpc}^{-1}$. This induces the so-called "circularity problem". This problem has been completely overcome for the first time by Dainotti et al. (2022a) for GRBs, and Dainotti et al. (2022h) and Lenart et al. (2023) for QSOs, which have analyzed the trend of k as a function of the cosmological model assumed a-priori. More precisely, in these studies, k is determined not by fixing the cosmological parameters of the assumed model, but over a grid of values of the cosmological parameters (i.e. Ω_M , H_0 , and also others for models different from the flat Λ CDM one), leading to the determination of the functions $k(\Omega_M)$ and $k(H_0)$. Even if k does not depend on H_0 , it shows a dependence on Ω_M and thus $k(\Omega_M)$ can be applied in the cosmological fits leaving k varies along with the free cosmological parameters, without fixing any cosmology a-priori. We have here described also this method for accounting for the redshift evolution since it is the most appropriate one to avoid the circularity problem. However, in this work we cannot apply this cosmology-independent correction, but only the "fixed" correction, in which we assume a specific cos-

¹ <https://github.com/PantheonPlusSH0ES>

mological model. Indeed, we are not dealing with cosmological fits in which cosmological parameters are free to vary and hence we can let k vary with them, but we are investigating a cosmographic model, in which the only free cosmological parameter is H_0 , which does not affect k . Nevertheless, to provide a complete and comprehensive picture of our analysis, we consider four possible treatments of the redshift evolution: without correction and with “fixed” correction by assuming three different values of Ω_M , $\Omega_M = 0.3$, $\Omega_M = 0.1$, and $\Omega_M = 0.9$ (see Tables 1 and 3). The investigated value of 0.3 is justified as it is the one expected for the current matter density in the Universe from the latest observations (Scolnic et al. 2018; Brout et al. 2022). On the other hand, the values of $\Omega_M = 0.1$ and $\Omega_M = 0.9$ have been chosen as illustrative examples corresponding to the highest and lowest values, respectively, that k can assume if Ω_M ranges in the physically accepted interval between 0.1 and 0.9. Indeed, the function $k(\Omega_M)$ decreases with increasing Ω_M , as shown in Figure 5 of Dainotti et al. (2022a) for GRBs and in Figure 4 of Dainotti et al. (2022h) for QSOs. Thus, as anticipated above, we assume k fixed according to the chosen Ω_M value. We here stress that the reason for investigating these three cases of “fixed” correction is that, since we cannot apply the above-described technique for the correction for redshift evolution which is model-independent, we test how our results depend on the a-priori assumption of a cosmology. This provides an insight of the impact of our cosmological assumptions which is crucial to interpret the results and draw conclusions.

3.3 Cosmographic model

We here employ the cosmographic model firstly proposed by Bargiacchi et al. (2021), which is an implementation of the one already presented in Risaliti & Lusso (2019) and Lusso et al. (2019). It is an orthogonal polynomial expansion of the luminosity distance in terms of the logarithmic quantity $\log_{10}(1+z)$, where the notation “orthogonal” refers to the fact that the coefficients of this power series are not correlated among each other. The uncorrelation between the coefficients of different orders is the main strength of this cosmographic approach since it implies that changing the maximum order of the polynomial does not modify the values of the coefficients of the retained orders. For example, if we move from a fourth-order polynomial to a fifth-order polynomial, the values of the coefficients of the first, second, third, and fourth orders would remain the same compared to the ones of the fourth-order expression. This also implies that, since each value of the coefficients is not correlated to the values of the other coefficients, we can check if an additional higher order in the expansion significantly deviates from zero and thus is needed in the polynomial. Moreover, to quantify the tension between the best-fit of the cosmographic model and the prediction of the flat Λ CDM model, this feature of orthogonality allows us to determine this discrepancy between the parameters we would obtain from the cosmographic approach and the ones expected from the cosmological model. This can be achieved without the need for accounting for the covariance among the free parameters of the cosmographic model.

As anticipated, the functional form of our cosmographic model simply allows us to determine which is the maximum order of the expansion needed in our study, the latter depending on the data set used. This can be clearly explained if we write down the form of the orthogonal logarithmic polynomial. If we consider a fifth-order

expansion, the luminosity distance can be written as²:

$$D_L(z) = \frac{c \ln(10)}{H_0} \left\{ \log_{10}(1+z) + a_2 \log_{10}^2(1+z) + a_3 \left[k_{32} \log_{10}^2(1+z) + \log_{10}^3(1+z) \right] + a_4 \left[k_{42} \log_{10}^2(1+z) + k_{43} \log_{10}^3(1+z) + \log_{10}^4(1+z) \right] + a_5 \left[k_{52} \log_{10}^2(1+z) + k_{53} \log_{10}^3(1+z) + k_{54} \log_{10}^4(1+z) + \log_{10}^5(1+z) \right] \right\}. \quad (9)$$

The first term, $\frac{c \ln(10)}{H_0}$, where c is the speed of light, and $a_1 = 1$ are imposed to recover the Hubble law at low z , which is $D_L(z) = \frac{c \ln(1+z)}{H_0}$. The coefficients k_{ij} are not free parameters, and depend on the probes considered and, especially, on their redshift distribution. Indeed, their values are determined through the following step-by-step procedure such that all the a_i in Eq. (9) are uncorrelated (for visualization see Figs. 1, 2, 3, and 4). This technique is completely general, it can be applied to any probe, and it should be performed any time the sample investigated changes.

As a first step, the considered data set is fitted with a second-order non-orthogonal polynomial $P_2 = \frac{c \ln(10)}{H_0} \left[\log_{10}(1+z) + a'_2 \log_{10}^2(1+z) \right]$ to obtain a'_2 . Then, the fit is performed with a

third-order non-orthogonal polynomial $P_3 = \frac{c \ln(10)}{H_0} \left[\log_{10}(1+z) + a''_2 \log_{10}^2(1+z) + a''_3 \log_{10}^3(1+z) \right]$ to determine a''_2 and a''_3 . By

comparing the orthogonal and non-orthogonal polynomial expressions we obtain the constraint $a''_2 = a'_2 + a''_3 k_{32}$. We apply the same procedure to the other order polynomials. Moving forward with the

fourth-order non-orthogonal polynomial $P_4 = \frac{c \ln(10)}{H_0} \left[\log_{10}(1+z) + a'''_2 \log_{10}^2(1+z) + a'''_3 \log_{10}^3(1+z) + a'''_4 \log_{10}^4(1+z) \right]$ we obtain a'''_2 , a'''_3 , and a'''_4 , and with the fifth-order non-orthogonal poly-

nomial $P_5 = \frac{c \ln(10)}{H_0} \left[\log_{10}(1+z) + a''''_2 \log_{10}^2(1+z) + a''''_3 \log_{10}^3(1+z) + a''''_4 \log_{10}^4(1+z) + a''''_5 \log_{10}^5(1+z) \right]$ we determine a''''_2 , a''''_3 , a''''_4 , and a''''_5 . Hence we impose the following equivalences:

$$a''_2 = a'_2 + a''_3 k_{32} + a'''_4 k_{42}, \quad (10)$$

$$a'''_3 = a''_3 + a'''_4 k_{43}, \quad (11)$$

$$a''''_2 = a'_2 + a''_3 k_{32} + a'''_4 k_{42} + a''''_5 k_{52}, \quad (12)$$

$$a''''_3 = a''_3 + a'''_4 k_{43} + a''''_5 k_{53}, \quad (13)$$

$$a''''_4 = a'''_4 + a''''_5 k_{54}. \quad (14)$$

The solutions to this system of equations are the six unknown coefficients k_{ij} . The same procedure can be straight-forwardly employed

² For sake of simplicity we use \ln instead of \log_e .

to determine k_{ij} for the logarithmic orthogonal polynomial of any order (greater or lower than the fifth order). We refer to [Bargiacchi et al. \(2021\)](#) for further detail on the overall procedure.

From Eq. (9) it is clearly visible that the higher-order coefficients become significant only at high redshifts. It means that the higher is the maximum redshift reached by the probes in our data set and the larger is the number of sources at high redshifts in our sample, and the higher is the maximum order of the polynomial needed to fit the cosmographic model. As a consequence, in our study, we have separately considered the two data sets used, QSOs alone and QSOs combined with GRBs, SNe Ia, and BAOs, to identify the proper polynomial expansion to be employed in the two different cases. As anticipated in Section 1, the flexibility of this cosmographic approach, that allows us to choose the most suitable functional form for the data investigated, guarantees an accurate fit of our data. We here also stress that the cosmographic approach we employ has already been validated in [Bargiacchi et al. \(2021\)](#) against possible issues such as convergence problems when the cosmographic function is fitted over a redshift range wider than its convergence radius, or troubles in the comparison between a cosmographic fit on the whole redshift range and the theoretical prediction of a given physical model, which is instead computed around $z = 0$ (see also Section 3.4).

3.4 Comparison with a flat Λ CDM model

As anticipated in Section 1 and detailed in [Bargiacchi et al. \(2021\)](#), to quantify the discrepancy between the cosmographic fit and a flat Λ CDM model, we can compare the best-fit values of the a_i coefficients in Eq. (9) (or for any order of the orthogonal polynomial logarithmic expansion of $D_L(z)$) to the one predicted in a flat Λ CDM model. To this end, we need to expand in power series of z both Eq. (9) and the expression of $D_L(z)$ in a flat Λ CDM model, which is

$$D_{L,\text{flat}\Lambda\text{CDM}}(z) = (1+z) \frac{c}{H_0} \int_0^z \frac{dz'}{\sqrt{\Omega_M(1+z')^3 + (1-\Omega_M)}}, \quad (15)$$

. Then, comparing the coefficients of the corresponding orders of the two obtained expansions, we obtain the required equations that link the cosmographic parameters to the cosmological ones. The relations between the free parameters a_i of the fourth-order cosmographic logarithmic expansion and Ω_M in a flat Λ CDM model are the following:

$$a_4 = \ln^3(10) \left(-\frac{135}{64} \Omega_M^3 + \frac{18}{4} \Omega_M^2 - \frac{47}{16} \Omega_M + \frac{5}{8} \right), \quad (16a)$$

$$a_3 = -k_{43} a_4 + \ln^2(10) \left(\frac{9}{8} \Omega_M^2 - 2\Omega_M + \frac{7}{6} \right), \quad (16b)$$

$$a_2 = -k_{32} a_3 - k_{42} a_4 + \ln(10) \left(-\frac{3}{4} \Omega_M + \frac{3}{2} \right). \quad (16c)$$

Extending to the fifth-order we obtain:

$$a_5 = \ln^4(10) \left(\frac{567}{128} \Omega_M^4 - \frac{729}{64} \Omega_M^3 + \frac{315}{32} \Omega_M^2 - \frac{25}{8} \Omega_M + \frac{31}{120} \right), \quad (17a)$$

$$a_4 = -k_{54} a_5 + \ln^3(10) \left(-\frac{135}{64} \Omega_M^3 + \frac{18}{4} \Omega_M^2 - \frac{47}{16} \Omega_M + \frac{5}{8} \right), \quad (17b)$$

$$a_3 = -k_{53} a_5 - k_{43} a_4 + \ln^2(10) \left(\frac{9}{8} \Omega_M^2 - 2\Omega_M + \frac{7}{6} \right), \quad (17c)$$

$$a_2 = -k_{32} a_3 - k_{42} a_4 - k_{52} a_5 + \ln(10) \left(-\frac{3}{4} \Omega_M + \frac{3}{2} \right). \quad (17d)$$

Tables 1 and 2 show, respectively, the best-fit a_i values and the predicted a_i values in a flat Λ CDM model under the different assumptions considered in this work when only QSOs are considered. Tables 3 and 4 report the same, but for all probes together.

3.5 Likelihoods and fitting procedure

The cosmographic fits presented in this work are performed with the Kelly method ([Kelly 2007](#)) in which all parameters are free to vary contemporaneously. Indeed, when considering QSOs alone (see Figs. 1 and 2), we fit the parameters of the RL relation, g_1 , n_1 , and sv_1 , the coefficients a_i of the cosmographic model, and H_0 , which is included in the cosmographic expansion of Eq. (9). Instead, when joining QSOs, GRBs, SNe Ia, and BAOs, we deal with the additional free parameters of the 3D relation, a , b , and sv (see Figs. 3 and 4). In both cases, we impose wide uniform priors on all free parameters. As already discussed in [Dainotti et al. \(2023c\)](#), to guarantee the reliability of the posterior distributions of the fitted parameters, we have employed the Gelman-Rubin convergence diagnostic test, which relies on the square root of the ratio between the variance intra-chain (within each chain) and the variance inter-chain (between one chain and another) (R), which is applied as a convergence probe: if R is large the convergence has not yet been reached. Following [Lenart et al. \(2023\)](#), [Bargiacchi et al. \(2023\)](#), and [Dainotti et al. \(2023c\)](#), we impose $R - 1 < 0.05$ to guarantee the convergence of each free parameter, which is more restrictive than $R - 1 < 0.1$ often required in the literature ([Dainotti et al. 2022h](#)).

In our analysis, we not only distinguish between our two different data sets (i.e. QSOs alone and the combination of QSOs, GRBs, SNe Ia, and BAOs), but also between the application of different likelihoods. Indeed, [Dainotti et al. \(2023b\)](#), [Dainotti et al. \(2023b\)](#), [Bargiacchi et al. \(2023\)](#), and [Dainotti et al. \(2023c\)](#) have proved through several statistical tests that the proper best-fit likelihoods for the samples here studied of QSOs, SNe Ia, and BAOs are not the commonly used Gaussian likelihoods, while they are a logistic for QSOs and a student-T for *Pantheon+* SNe Ia and BAOs. Only GRBs from the Platinum sample are properly fitted through a Gaussian likelihood. The above-mentioned works have also shown the importance of choosing the proper likelihood for each probe to significantly reduce the uncertainties on the fitted parameters. We here stress that the newly found distributions do not effectively reveal the truth about underlying likelihoods of QSOs, SNe Ia, and BAOs but they reproduce the actual distributions of these probes better than the commonly used Gaussian distribution. In this sense, the new best-fit distributions represent a useful and more precise parameterization to constrain parameters with increased accuracy, as shown in [Bargiacchi et al. \(2023\)](#), [Dainotti et al. \(2023c\)](#), and [Dainotti et al. \(2023b\)](#). Hence, in this work we separately consider the cases in which the data sets (QSOs alone or the combination of all four probes) are fitted with Gaussian likelihoods ($\mathcal{L}_{\text{Gaussian}}$) and with the new best-fit proper likelihoods (\mathcal{L}_{new}). When fitting all probes together, we employ the joint likelihood, as discussed in detail in [Dainotti et al. \(2023c\)](#), and, in the case of \mathcal{L}_{new} we consider as an additional free parameter the degree of freedom of the student-T distribution, ν_{SNe} and ν_{BAO} , for SNe Ia and BAOs respectively, as shown in Figure 4.

3.5.1 The posterior likelihood

We here detail the posterior likelihood mentioned above. Indeed, the posterior probability is obtained as the sum (or the product if we consider the natural logarithm units) of the prior probability and the

likelihood. As stated before, we impose a uniform (i.e. uninformative) prior on all free parameters in the following wide ranges: $0.1 < g_1 < 1$, $2 < n_1 < 20$, $0 < sv_1 < 2$, $50 \text{ km s}^{-1} \text{ Mpc}^{-1} \leq H_0 \leq 100 \text{ km s}^{-1} \text{ Mpc}^{-1}$, $-100 \leq a_2 \leq 150$, $-100 \leq a_3 \leq 150$, $-100 \leq a_4 \leq 150$, $-100 \leq a_5 \leq 150$, and, when also GRBs, SNe Ia, and BAOs are considered, $0 < v_{\text{SNe}} < 10$, $0 < v_{\text{BAO}} < 10$, $-2 < a < 0$, $0 < b < 2$, and $0 < sv < 2$. Concerning the likelihoods, when we investigate $\mathcal{L}_{\text{Gaussian}}$, the likelihood is defined for each individual probe as follows, where \ln stands for the natural logarithm and \mathcal{L} for the likelihood. For QSOs,

$$\ln(\mathcal{L})_{\text{QSOs}} = -\frac{1}{2} \sum_{i=1}^N \left[\frac{(\log_{10} L_{X,obs,i} - \log_{10} L_{X,th,i})^2}{\hat{s}_i^2} + \ln(\hat{s}_i^2) \right] \quad (18)$$

where $\hat{s}_i^2 = \sigma_{\log_{10} L_{X,obs,i}}^2 + g_1^2 \sigma_{\log_{10} L_{UV,obs,i}}^2 + sv_1^2$ in which the statistical uncertainties on $\log_{10} L_{X,obs}$ and $\log_{10} L_{UV,obs}$ and the intrinsic dispersion sv_1 are taken into account. Similarly, for GRBs,

$$\ln(\mathcal{L})_{\text{GRBs}} = -\frac{1}{2} \sum_{i=1}^N \left[\frac{(\mu_{obs,GRBs,i} - \mu_{th,i})^2}{s_i^2} + \ln(s_i^2) \right] \quad (19)$$

where $s_i^2 = \sigma_{\mu_{obs,GRBs}}^2 + sv^2$ which accounts for the statistical uncertainties on the measured quantities but also the intrinsic dispersion sv . For SNe Ia instead \mathcal{L} is built as

$$\ln(\mathcal{L})_{\text{SNeIa}} = -\frac{1}{2} \left[(\boldsymbol{\mu}_{obs,\text{SNeIa}} - \boldsymbol{\mu}_{th})^T C^{-1} (\boldsymbol{\mu}_{obs,\text{SNeIa}} - \boldsymbol{\mu}_{th}) \right] \quad (20)$$

where C is the covariance matrix that includes both statistical and systematic uncertainties on the measured distance moduli provided by *Pantheon+* release. In the case of BAOs, \mathcal{L} reads as

$$\ln(\mathcal{L})_{\text{BAO}} = -\frac{1}{2} \left[(d_{z,obs} - d_{z,th})^T C^{-1} (d_{z,obs} - d_{z,th}) \right] \quad (21)$$

with C the covariance matrix provided in Sharov (2016).

On the other hand, when applying the new best-fit likelihoods \mathcal{L}_{new} , the formula for GRBs remains unchanged (Eq. (19)) since the likelihood is still Gaussian, while for the other probes we need to employ the actual probability distribution functions (PDFs). Hence, in the case of QSOs \mathcal{L} follows from a logistic PDF and reads as:

$$\ln(\mathcal{L})_{\text{QSOs}} = \ln(\text{PDF}_{\text{logistic}}) = \ln \frac{e^{-\frac{(\log_{10} L_{X,obs} - \log_{10} L_{X,th})}{\xi}}}{\xi \left(1 + e^{-\frac{(\log_{10} L_{X,obs} - \log_{10} L_{X,th})}{\xi}} \right)^2}, \quad (22)$$

where ξ is the scale parameter for which $\hat{s}^2 = (\xi^2 \pi^2)/3$. Similarly, we replace Eqs. (20) and (21) with the likelihoods obtained from a student-T PDF. Thus, for SNe Ia

$$\begin{aligned} \ln(\mathcal{L})_{\text{SNeIa}} &= \ln(\text{PDF}_{\text{student}}) = \\ &= \ln \frac{\Gamma\left(\frac{v_{\text{SNe}}+1}{2}\right)}{\sqrt{v_{\text{SNe}}} \pi \xi \Gamma\left(\frac{v_{\text{SNe}}}{2}\right)} \left[1 + \frac{((\boldsymbol{\mu}_{obs,\text{SNeIa}} - \boldsymbol{\mu}_{th})/\xi)^2}{v_{\text{SNe}}} \right]^{-\frac{v_{\text{SNe}}+1}{2}}, \end{aligned} \quad (23)$$

where Γ is the γ function and the variance is $\sigma^2 = (\xi^2 v_{\text{SNe}})/(v_{\text{SNe}} - 2)$. Instead, considering BAOs:

$$\begin{aligned} \ln(\mathcal{L})_{\text{BAO}} &= \ln(\text{PDF}_{\text{student}}) = \\ &= \ln \frac{\Gamma\left(\frac{v_{\text{BAO}}+1}{2}\right)}{\sqrt{v_{\text{BAO}}} \pi \xi \Gamma\left(\frac{v_{\text{BAO}}}{2}\right)} \left[1 + \frac{((d_{z,obs} - d_{z,th})/\xi)^2}{v_{\text{BAO}}} \right]^{-\frac{v_{\text{BAO}}+1}{2}}, \end{aligned} \quad (24)$$

where the variance is $\sigma^2 = (\xi^2 v_{\text{BAO}})/(v_{\text{BAO}} - 2)$.

We here stress that, as anticipated in Sect. 3.5, when combining all the probes, we use the joint likelihood, that is the sum of all the $\ln \mathcal{L}$ above-defined (see Dainotti et al. 2023c, for details). This joint likelihood (or only the one of QSOs when QSOs alone are used) is then added to the natural logarithm of the prior probability to obtain the posterior likelihood.

4 RESULTS AND DISCUSSION

4.1 Results from QSOs alone

We here outline the results obtained by fitting QSOs alone.

- The first step in our cosmographic procedure is to determine the order of the orthogonal logarithmic polynomial that is required to properly fit the data. As detailed in Section 3.3, the maximum order needed depends on the sample considered. When using only QSOs, we obtain that the fifth-order is negligible, since in all cases studied the best-fit value of a_5 is consistent with 0 within much less than 1σ . Hence, we truncate the formula of Eq. (9) to the fourth order imposing $a_5 = 0$. Indeed, as visible from Table 1 and Figs. 1 and 2, a_4 is significant since it is always discrepant from $a_4 = 0$ at $> 1 \sigma$ level.

- Comparing the results from the different likelihoods in Table 1, we can observe that \mathcal{L}_{new} leads to reduced uncertainties on the parameters compared to $\mathcal{L}_{\text{Gaussian}}$, as already proved in the cosmological analyses of Dainotti et al. (2023b), Bargiacchi et al. (2023), and Dainotti et al. (2023c). More specifically, in our case \mathcal{L}_{new} in general lowers the errors on the higher-order a_i coefficients, reaching a reduction of $\sim 23\%$. Nevertheless, QSOs alone cannot yield tight constraints on the coefficients a_i , which are indeed associated with large 1σ uncertainties.

- Concerning instead the only cosmological parameters, H_0 , it is not constrained in any of the cases studied with QSOs alone, as shown in Figs. 1 and 2. Indeed, QSOs alone not calibrated on SNe Ia, which behave as anchors for the low- z regime, cannot determine H_0 , as already discussed in Dainotti et al. (2023c).

- For both the likelihoods considered, a trend between the three cases (i.e. $\Omega_M = 0.3$, $\Omega_M = 0.1$, and $\Omega_M = 0.9$) with fixed correction for evolution and the case without correction is exhibited: the application of the correction leads to higher uncertainties of a_i since the evolutionary parameter k brings an additional uncertainty. Moreover, the cases with correction significantly changes the best-fit values of the coefficients compared to the ones obtained without the correction for the evolution. We can also notice that the case with correction with $\Omega_M = 0.9$ is the one that leads to best-fit values more similar to the ones obtained without evolution. This is completely in agreement with Lenart et al. (2023), where it is shown that QSOs alone, without calibration on SNe Ia and without accounting for any correction for the redshift evolution, prefer Ω_M towards 0.9 (see their Table 2 and Figure 7). Indeed, these two configurations, the one

without correction and the one with correction and $\Omega_M = 0.9$, are the ones that bring the lowest uncertainties on a_2 , a_3 , and a_4 .

- Focusing on the best-fit values of the a_i coefficients, as anticipated, we obtain very discrepant values comparing the different evolutionary cases for each likelihood studied, even though also the uncertainties are large. When comparing instead the best-fit values of the coefficient of the same order for $\mathcal{L}_{Gaussian}$ and \mathcal{L}_{new} and same cases of evolutionary correction, we notice that all a_i are consistent within less than 1σ , thus the two likelihoods yield compatible best-fit values, in agreement with the results of Bargiacchi et al. (2023) and Dainotti et al. (2023c).

- Through Eqs. (16), we compute the discrepancy between the obtained best-fit values of a_i reported in Table 1 and the theoretically predicted values in a flat Λ CDM model (Table 2) for the same cases. There is only one case of compatibility within 1σ : a_3 with correction for redshift evolution with $\Omega_M = 0.9$ for both likelihoods. More precisely, in this case we obtain compatibility in 0.3σ and 0.4σ , for $\mathcal{L}_{Gaussian}$ and \mathcal{L}_{new} , respectively. In all the other cases studied, a tension with the flat Λ CDM model emerges with a significance level $> 1 \sigma$, that reaches up to $\sim 14 \sigma$ on a_2 in the case without correction for redshift evolution for both the likelihoods.

4.2 Results from all probes together

As already discussed in detail in Bargiacchi et al. (2022) and Dainotti et al. (2023c), a debate has recently emerged on the importance of properly combining data sets that do not reveal manifest tension to infer correct statistical interpretations from the analyses (Planck Collaboration et al. 2020; Efstathiou & Gratton 2020; Vagnozzi et al. 2021; Gonzalez et al. 2021). In this regard, QSOs pose a problem since, as standalone probes, determine parameters with no tight constraints and large uncertainties, as stressed above. Thus, to assess the combination of QSOs with other probes and to verify if all the probes can be joint, in future studies, we would need to strongly reduce the intrinsic dispersion of the RL relation such that QSOs could reach the precision of SNe Ia in constraining parameters as it has been already done in Dainotti et al. (2023a). The aim here however is to understand to what extend the total sample of QSOs adopted for cosmological analyses can indeed be used in the cosmographic approach. Future studies may entail the use of cosmographic applications with this golden sample. Beside the relevance of this topic, it is beyond the aim of our analysis, and we here discuss the results obtained by combining QSOs, GRBs, SNe Ia, and BAOs, analyzing the different cases studied, the difference and similarities with the results from QSOs alone, and comparing with previous works in the literature.

- Starting from the maximum order of the orthogonal logarithmic polynomial needed to fit all probes together, we notice from Table 3 and Figs. 3 and 4 that in all the cases with $\mathcal{L}_{Gaussian}$ a_5 is significant with a discrepancy from $a_5 = 0$ always greater than 1.5σ . We have further checked that instead the addition of the sixth-order leads to a_6 compatible with $a_6 = 0$. Hence, in this cases we have used the fifth-order function, as in Eq. (9). The discrepancy of a_5 from 0 appears to be reduced when using \mathcal{L}_{new} , reaching the minimum of 0.2σ in the case with the correction for evolution applied by assuming $\Omega_M = 0.9$. This shows that the use of \mathcal{L}_{new} , in place of $\mathcal{L}_{Gaussian}$, reduces the dimensionality of the cosmographic polynomial. Nevertheless, we still fit a fifth-order cosmographic model (Eq. (9)) when applying \mathcal{L}_{new} to be consistent with the case of $\mathcal{L}_{Gaussian}$. As already stated for QSOs alone, we can also notice that \mathcal{L}_{new} reduce the uncertainties on the parameters compared to $\mathcal{L}_{Gaussian}$, mainly on

the higher-order coefficients, up to a maximum reduction of $\sim 20\%$, and on H_0 , with an uncertainty reduced of $\sim 28\%$. This reduction on the error on H_0 obtained through \mathcal{L}_{new} confirms the results of Dainotti et al. (2023b) and Dainotti et al. (2023c).

- Still focusing on H_0 , we observed that, differently from the case of only QSOs, the combination of the four probes allows us to obtain close contours on H_0 in all cases studied. The value of H_0 is always around $73 \text{ km s}^{-1} \text{ Mpc}^{-1}$ within 0.5σ , since it is mainly driven by *Pantheon+* SNe Ia and BAOs (see e.g. Riess et al. 2022; Dainotti et al. 2022a; Bargiacchi et al. 2023; Dainotti et al. 2023c), and it is in all cases compatible within 0.5σ with the value $H_0 = 73.04 \pm 1.04$ reported in Riess et al. (2022). In addition, the use of \mathcal{L}_{new} slightly lowers the value of H_0 if we compare corresponding cases for the treatment of the redshift evolution.

- Independently on the likelihood, we can identify, similar to the case of only QSOs, a trend between the three cases with fixed correction for evolution and the case without correction. Indeed, the inclusion of the correction leads to higher uncertainties of the coefficients a_i of the highest orders (mainly a_4 and a_5), due to the fact that also the additional uncertainties on the evolutionary parameters are taken into account. Moreover, since the correction for the redshift evolution affects more the high redshifts, the cases in which this correction is applied lead to best-fit values of the highest coefficients significantly discrepant from the ones obtained without accounting for the correction for the evolution. However, this discrepancy is partially alleviated by the large errors on the a_i of the highest orders. From the point of view of this comparison between cases with and without correction, it is also visible that among the different applications of the correction for the redshift evolution, the one that assumes $\Omega_M = 0.9$ is the one closer, in terms of best-fit values, to the case without evolution, as outlined in the case of QSOs alone. Once again, these two cases are the ones which lead to the lowest uncertainties on a_3 , a_4 , and a_5 .

- Concerning the a_i coefficients, we obtain best-fit values of a_2 compatible within 1σ among all evolutionary cases for each likelihood studied, while a_3 , a_4 , and a_5 show discrepancies among each other at different significance levels when comparing different treatments of the redshift evolution. Indeed, this discrepancy reaches a maximum of 5.7σ and 7σ , for a_4 with $\mathcal{L}_{Gaussian}$ and \mathcal{L}_{new} , respectively between the cases without correction and with correction and $\Omega_M = 0.1$. Similarly, if we compare the cases without correction and with correction and $\Omega_M = 0.3$, the maximum discrepancy is obtained for a_4 at a significance level of 4.1σ and 5.3σ , with $\mathcal{L}_{Gaussian}$ and \mathcal{L}_{new} , respectively. For the cases without correction and with correction and $\Omega_M = 0.9$, a_4 shows a discrepancy, which is of 3σ and 3.8σ , with $\mathcal{L}_{Gaussian}$ and \mathcal{L}_{new} , respectively. When comparing instead the best-fit values of the coefficients a_i of the same order for the two different likelihoods and the same evolutionary corrections, we observe that a_3 , a_4 , and a_5 are compatible within 1σ , while a_2 shows a discrepancy $\geq 4 \sigma$, also due to the lower uncertainties on a_2 compared to the ones of the other coefficients.

- Following Eqs. (17), we can also quantify the tension with the prediction of a flat Λ CDM model by comparing the best-fit a_i values in Table 3 with the values reported in Table 4 for the corresponding cases. The only cases in which the obtained values are compatible within 1σ with the theoretical predictions are the following: a_4 in the case of correction for redshift evolution with $\Omega_M = 0.9$ and $\mathcal{L}_{Gaussian}$ (at 0.9σ level), a_4 and a_5 in the case of correction for redshift evolution with $\Omega_M = 0.9$ and \mathcal{L}_{new} (at 0.8 and 0.1σ level respectively). All the other cases manifest a tension with the flat Λ CDM model $\geq 1 \sigma$, reaching a maximum discrepancy $> 30 \sigma$

on a_2 in the case of correction for redshift evolution with $\Omega_M = 0.9$ for both the likelihoods.

- Based on the previous points, we can now compare our results to previous works in the literature that apply QSOs in cosmography together with other probes. In this regard, [Lusso et al. \(2019\)](#) used a less updated sample of 1598 QSOs between $z = 0.04$ and $z = 5.1$, SNe Ia from the *Pantheon sample* ([Scolnic et al. 2018](#)), and 162 GRBs in the range $z = 0.03 - 6.67$ standardized through the Amati relation. In [Lusso et al. \(2019\)](#) work, the cosmographic model is a fourth-order non-orthogonal logarithmic polynomial and only the Gaussian likelihood is employed without any correction for the redshift evolution of luminosities of QSOs and GRBs. Beside these differences, they still found a strong overall discrepancy ($> 4\sigma$) with a flat Λ CDM with $\Omega_M = 0.3$. Moreover, in our study, thank to the orthogonalization of the cosmographic polynomial, we reduce the uncertainties on a_2 , a_3 , and a_4 compared to [Lusso et al. \(2019\)](#).

The same cosmographic model (Eq. (9)) as in our study, was instead already applied in [Bargiacchi et al. \(2021\)](#), where *Pantheon* SNe Ia were combined to the QSO sample used here but with only sources at $z > 0.7$. In [Bargiacchi et al. \(2021\)](#) analysis, only the case without correction for evolution, with Gaussian likelihood, and with H_0 fixed to $70 \text{ km s}^{-1} \text{ Mpc}^{-1}$ was considered. As in [Lusso et al. \(2019\)](#), the cosmographic fit of [Bargiacchi et al. \(2021\)](#) revealed a discrepancy $> 4\sigma$ with a flat Λ CDM with $\Omega_M = 0.3$. Comparing corresponding cases at $\Omega_M = 0.3$, besides the differences in the data set and the analysis, we find compatibility within 1σ between our best-fit a_i values and the ones reported in [Bargiacchi et al. \(2021\)](#). This confirms the overall outcome of the cosmographic analysis, but we here stress that our work presents important points of novelty: the combination of the most updated samples of probes, the use of the QSO sample in the whole redshift range of observations which leverages also on low-redshift sources, the correction for redshift evolution and selection biases, and the employment of the best-fit likelihoods (\mathcal{L}_{new}). All these new points, combined together, proved to be crucial to better constrain the cosmographic model, thus providing a more precise description of the Universe, which is completely model-independent, and an improved estimate of the tension with the flat Λ CDM model.

5 CONCLUSIONS

In this work, we have performed a completely model-independent test of the flat Λ CDM model leveraging the advantages of the robust cosmographic technique developed in [Bargiacchi et al. \(2021\)](#), which is based on an orthogonal logarithmic polynomial of the luminosity distance. We have applied this procedure both to QSOs alone and to the combination of QSOs, GRBs, SNe Ia, and BAOs. In both cases we have also accounted for different treatments of the likelihoods ([Bargiacchi et al. 2023](#); [Dainotti et al. 2023c,b](#)), and selection biases and redshift evolution of the luminosities of QSOs and GRBs ([Dainotti et al. 2013a, 2015, 2017a, 2021a, 2022a](#); [Bargiacchi et al. 2023](#); [Dainotti et al. 2023c, 2022h](#); [Lenart et al. 2023](#); [Bargiacchi et al. 2023](#); [Dainotti et al. 2023c](#); [Dainotti et al. 2023a](#)). Indeed, we have distinguished four approaches for the correction for redshift evolution, one without correction and three different cases of correction when Ω_M is fixed to 0.1, 0.3 and 0.9, and two approaches for the likelihoods, one with the traditional Gaussian and another one with the recently found best-fit likelihoods for each probe. Our comprehensive analysis leverages the cosmology independence of cosmography, the invaluable role of high-redshift sources, such as QSOs and GRBs, which are able to unveil tensions between the observed data and the predictions of cosmological models, and the

power of low-redshift probes, such as SNe Ia and BAOs, which lead to an increased precision in the determination of the cosmological parameters.

Our study shows that QSOs alone still needs to be improved, at least for the total sample of 2421 sources here presented, compared to the combination of all probes, leading to large uncertainties on the cosmographic free parameters and a H_0 not constrained. Nonetheless, they provide a coverage of the high redshift range that brings crucial information on the evolution of the Universe and thus on the discrepancies with cosmological models pointing toward a tension with the flat Λ CDM model. Once QSOs are combined with GRBs, SNe Ia, and BAOs, all parameters are better constrained and H_0 , driven by SNe Ia and BAOs, is in all cases compatible with the most recent value reported in [Riess et al. \(2022\)](#). Both when dealing with only QSOs and with all probes together, the inclusion of the correction for redshift evolution significantly changes the results, while the application of \mathcal{L}_{new} strongly reduces the uncertainties on parameters compared to $\mathcal{L}_{Gaussian}$, leading to a maximum reduction on H_0 of $\sim 28\%$. This marks the importance of accounting for the redshift evolution and the best-fit likelihood to obtain the actual best-fits with better constraints. These results of better constraining the cosmographic parameters is indeed aligned with the reduction of the scatter we have on the cosmological parameters when we use the \mathcal{L}_{new} . These results also stress the importance of these new likelihoods both in the cosmology and cosmographic domain. Finally, in all the cases investigated, we have obtained an overall discrepancy between the data and the flat Λ CDM model, which in some cases reaches a statistical significance, in agreement with previous cosmographic studies ([Lusso et al. 2019](#); [Bargiacchi et al. 2021](#)). On the other hand, the tension achieved in this work reaches a statistical level much higher than the ones obtained in cosmological studies which use the combination of QSOs, GRBs, SNe Ia, and BAOs, such as [Bargiacchi et al. \(2023\)](#) and [Dainotti et al. \(2023c\)](#). Specifically, [Bargiacchi et al. \(2023\)](#) have investigated the flat Λ CDM model, while [Dainotti et al. \(2023c\)](#) have extended the analysis to the non-flat Λ CDM and flat w CDM model. Thus, the fact that in this study the tension proves to be increased, compared to those works, means that the cosmographic model points toward a cosmological model different (especially phantom model, [Lenart et al. 2023](#)) to the ones already investigated. Another important point to be taken into account is that in this treatment, differently from the cosmological approach, we cannot apply the evolutionary function which changes at the change of Ω_M ([Lenart et al. 2023](#); [Bargiacchi et al. 2023](#); [Dainotti et al. 2023c](#)) and prevents the values of Ω_M to be closer to 1. Thus, if a cure to this effect could indeed be used, the values of Ω_M would be shifted at smaller values and we envision the discrepancy could be smaller. In conclusion, we have demonstrated the power of the cosmographic approach embedded with high-redshift probes, once they are carefully corrected for biases and redshift evolution and the proper likelihoods are employed.

In this scenario, without any specific cosmological assumption, a tension has emerged between the observations and the theoretical prediction of the flat Λ CDM model, making the hunt for the most suitable description of the Universe even more puzzling along with the quest of the reasons for these discrepancies.

ACKNOWLEDGEMENTS

GB acknowledges Scuola Superiore Meridionale, for supporting her visit at NAOJ, Division of Science. GB thanks the Division of Science for being hosted on campus.

Table 1. Best-fit values of the a_i coefficients along with their 1σ uncertainty from QSOs alone for all cases investigated. H_0 is in units of $\text{km s}^{-1} \text{Mpc}^{-1}$, but it is not constrained by QSOs alone.

	$\mathcal{L}_{\text{Gaussian}}$				\mathcal{L}_{new}			
	a_2	a_3	a_4	H_0	a_2	a_3	a_4	H_0
No Evolution	1.12 ± 0.37	-2.83 ± 1.62	10.53 ± 6.31	74.73 ± 14.45	1.19 ± 0.38	-3.18 ± 1.56	11.38 ± 6.00	74.94 ± 15.50
Fixed Evolution ($\Omega_M = 0.3$)	10.23 ± 2.82	9.56 ± 2.19	29.70 ± 18.43	75.24 ± 14.51	13.64 ± 2.89	10.12 ± 2.04	27.30 ± 17.53	75.97 ± 14.45
Fixed Evolution ($\Omega_M = 0.1$)	8.50 ± 3.38	19.08 ± 3.27	52.57 ± 27.82	75.61 ± 14.49	13.86 ± 3.52	20.24 ± 3.14	48.56 ± 27.09	74.63 ± 14.35
Fixed Evolution ($\Omega_M = 0.9$)	11.57 ± 1.94	3.14 ± 2.39	21.59 ± 18.00	74.51 ± 14.59	12.61 ± 2.00	3.19 ± 2.09	17.53 ± 13.91	74.26 ± 14.22

Table 2. Values of a_i predicted in a flat Λ CDM model according to Eqs. (16) for only QSOs and all cases studied in this work.

	$\mathcal{L}_{\text{Gaussian}}$			\mathcal{L}_{new}		
	a_2	a_3	a_4	a_2	a_3	a_4
Flat Λ CDM, No Evolution	6.45	4.93	1.12	6.48	4.94	1.12
Flat Λ CDM, Fixed Evolution ($\Omega_M = 0.3$)	3.81	4.40	1.12	5.03	4.40	1.12
Flat Λ CDM, Fixed Evolution ($\Omega_M = 0.1$)	2.51	8.21	4.57	5.13	8.19	4.57
Flat Λ CDM, Fixed Evolution ($\Omega_M = 0.9$)	4.46	2.43	1.08	4.51	2.43	1.08

Table 3. Best-fit values of the a_i coefficients along with their 1σ uncertainty from all probes together for all cases investigated. H_0 is in units of $\text{km s}^{-1} \text{Mpc}^{-1}$.

	$\mathcal{L}_{\text{Gaussian}}$					\mathcal{L}_{new}				
	a_2	a_3	a_4	a_5	H_0	a_2	a_3	a_4	a_5	H_0
No Evolution	3.90 ± 0.05	2.40 ± 0.38	-9.40 ± 1.57	9.69 ± 5.83	73.19 ± 0.37	3.56 ± 0.04	2.57 ± 0.38	-7.89 ± 1.31	3.88 ± 5.60	72.77 ± 0.27
Fixed Evolution ($\Omega_M = 0.3$)	3.98 ± 0.05	5.37 ± 0.41	5.77 ± 2.13	22.17 ± 10.25	73.54 ± 0.38	3.59 ± 0.04	4.84 ± 0.36	8.63 ± 1.89	7.99 ± 8.70	73.11 ± 0.28
Fixed Evolution ($\Omega_M = 0.1$)	4.01 ± 0.05	5.56 ± 0.45	13.21 ± 2.42	35.76 ± 11.93	73.57 ± 0.39	3.63 ± 0.04	5.41 ± 0.38	16.85 ± 2.24	21.22 ± 10.19	73.16 ± 0.28
Fixed Evolution ($\Omega_M = 0.9$)	3.96 ± 0.05	4.37 ± 0.40	0.06 ± 1.88	13.59 ± 8.66	73.48 ± 0.37	3.62 ± 0.04	4.18 ± 0.32	3.00 ± 1.63	1.16 ± 6.96	73.06 ± 0.27

DATA AVAILABILITY

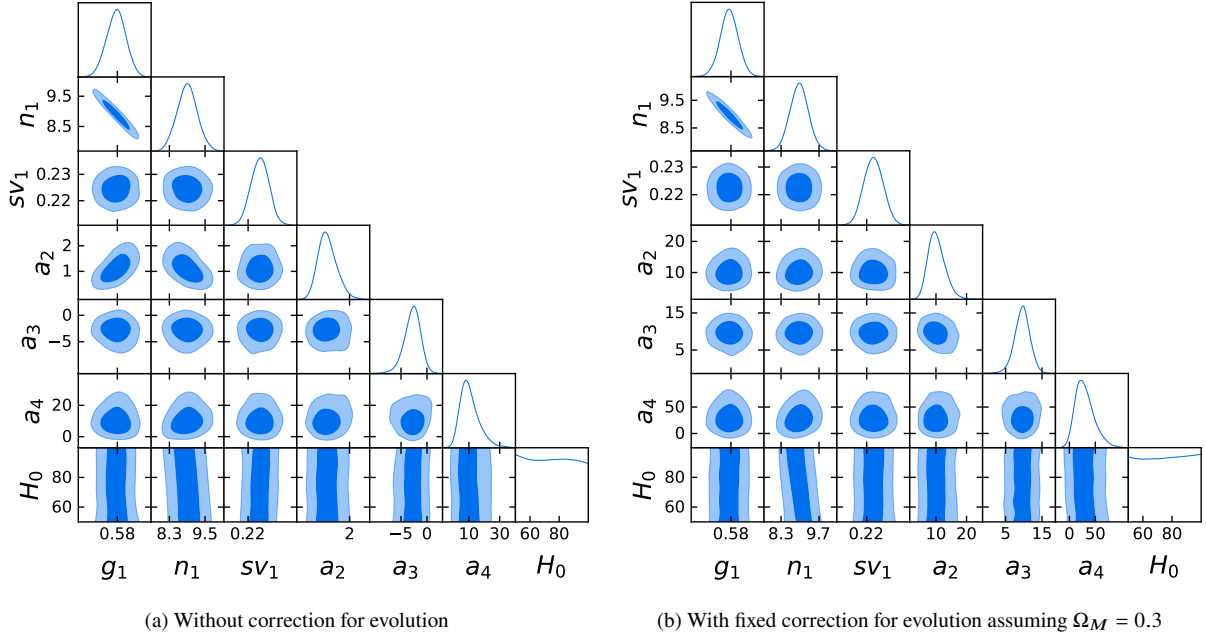
The data underlying this article will be shared upon a reasonable request to the corresponding author.

REFERENCES

- Aubourg É., et al., 2015, *Phys. Rev. D*, **92**, 123516
- Aviles A., Bravetti A., Capozziello S., Luongo O., 2014, *Phys. Rev. D*, **90**, 043531
- Avni Y., Tananbaum H., 1986, *ApJ*, **305**, 83
- Bargiacchi G., Risaliti G., Benetti M., Capozziello S., Lusso E., Saccardi A., Signorini M., 2021, *A&A*, **649**, A65
- Bargiacchi G., Benetti M., Capozziello S., Lusso E., Risaliti G., Signorini M., 2022, *MNRAS*, **515**, 1795
- Bargiacchi G., Dainotti M. G., Nagataki S., Capozziello S., 2023, *MNRAS*, Benetti M., Capozziello S., 2019, *JCAP*, **12**, 008
- Bernardini M. G., Margutti R., Zaninoni E., Chincarini G., 2012, *MNRAS*, **425**, 1199
- Beutler F., et al., 2011, *MNRAS*, **416**, 3017
- Bisogni S., Lusso E., Civano F., Nardini E., Risaliti G., Elvis M., Fabbiano G., 2021, *A&A*, **655**, A109
- Bloom J. S., Frail D. A., Sari R., 2001, *AJ*, **121**, 2879
- Brout D., et al., 2022, *ApJ*, **938**, 110
- Capozziello S., D'Agostino R., Luongo O., 2018, *MNRAS*, **476**, 3924
- Capozziello S., D'Agostino R., Luongo O., 2019, *International Journal of Modern Physics D*, **28**, 1930016
- Capozziello S., D'Agostino R., Luongo O., 2020, *MNRAS*, **494**, 2576
- Cardone V. F., Capozziello S., Dainotti M. G., 2009, *MNRAS*, **400**, 775
- Cardone V. F., Dainotti M. G., Capozziello S., Willingale R., 2010, *MNRAS*, **408**, 1181
- Carroll S. M., 2001, *Living Reviews in Relativity*, **4**, 1
- Colgáin E. Ó., Sheikh-Jabbari M. M., Solomon R., Bargiacchi G., Capozziello S., Dainotti M. G., Stojkovic D., 2022a, *arXiv e-prints*, p. [arXiv:2203.10558](https://arxiv.org/abs/2203.10558)
- Colgáin E. Ó., Sheikh-Jabbari M. M., Solomon R., Dainotti M. G., Stojkovic D., 2022b, *arXiv e-prints*, p. [arXiv:2206.11447](https://arxiv.org/abs/2206.11447)
- Cucchiara A., et al., 2011, *ApJ*, **736**, 7
- Cuceu A., Farr J., Lemos P., Font-Ribera A., 2019, *J. Cosmology Astropart. Phys.*, **2019**, 044
- Dainotti M. G., Amati L., 2018, *PASP*, **130**, 051001
- Dainotti M. G., Del Vecchio R., 2017, *New Astron. Rev.*, **77**, 23
- Dainotti M. G., Cardone V. F., Capozziello S., 2008, *MNRAS*, **391**, L79
- Dainotti M. G., Willingale R., Capozziello S., Fabrizio Cardone V., Ostrowski M., 2010, *ApJ*, **722**, L215
- Dainotti M. G., Fabrizio Cardone V., Capozziello S., Ostrowski M., Willingale R., 2011, *ApJ*, **730**, 135
- Dainotti M. G., Cardone V. F., Piedipalumbo E., Capozziello S., 2013a, *MNRAS*, **436**, 82
- Dainotti M. G., Petrosian V., Singal J., Ostrowski M., 2013b, *ApJ*, **774**, 157
- Dainotti M., Petrosian V., Willingale R., O'Brien P., Ostrowski M., Nagataki S., 2015, *MNRAS*, **451**, 3898
- Dainotti M. G., Postnikov S., Hernandez X., Ostrowski M., 2016, *ApJ*, **825**, L20

Table 4. Values of a_i predicted in a flat Λ CDM model according to Eqs. (17) for all probes together and all cases studied in this work.

	$\mathcal{L}_{Gaussian}$				\mathcal{L}_{new}			
	a_2	a_3	a_4	a_5	a_2	a_3	a_4	a_5
Flat Λ CDM, No Evolution	3.76	3.67	-0.85	-1.82	3.65	3.68	-0.91	-1.82
Flat Λ CDM, Fixed Evolution ($\Omega_M = 0.3$)	3.76	3.68	-0.55	-1.82	3.68	3.69	-0.52	-1.82
Flat Λ CDM, Fixed Evolution ($\Omega_M = 0.1$)	4.67	7.67	5.40	0.94	4.56	7.41	5.39	0.94
Flat Λ CDM, Fixed Evolution ($\Omega_M = 0.9$)	2.29	2.15	1.66	0.61	2.27	2.17	1.67	0.61

**Figure 1.** Fit of QSOs alone with $\mathcal{L}_{Gaussian}$ for the evolutionary cases without correction for evolution (left panel) and with fixed correction for evolution assuming $\Omega_M = 0.3$ (right panel). For sake of visualization clarity, we do not show also the other two cases of fixed correction with $\Omega_M = 0.1$ and $\Omega_M = 0.9$ investigated in this work. These additional cases present similarities to the ones here shown and are described in detail in Table 1 and discussed in Sect. 4.1.

Dainotti M. G., Nagataki S., Maeda K., Postnikov S., Pian E., 2017a, *A&A*, **600**, A98

Dainotti M. G., Hernandez X., Postnikov S., Nagataki S., O'brien P., Willingale R., Striegel S., 2017b, *ApJ*, **848**, 88

Dainotti M. G., Del Vecchio R., Tarnopolski M., 2018, *Advances in Astronomy*, **2018**, 4969503

Dainotti M., Lenart A., Sarracino G., Nagataki S., Capozziello S., Fraija N., 2020a, *ApJ*, **904**, 19

Dainotti M. G., Lenart A. L., Sarracino G., Nagataki S., Capozziello S., Fraija N., 2020b, *ApJ*, **904**, 97

Dainotti M. G., et al., 2020c, *ApJ*, **905**, L26

Dainotti M., Levine D., Fraija N., Chandra P., 2021a, *Galaxies*, **9**, 95

Dainotti M. G., et al., 2021b, *ApJS*, **255**, 13

Dainotti M. G., De Simone B., Schiavone T., Montani G., Rinaldi E., Lambiase G., 2021c, *ApJ*, **912**, 150

Dainotti M. G., Petrosian V., Bowden L., 2021d, *ApJ*, **914**, L40

Dainotti M. G., Sarracino G., Capozziello S., 2022b, *PASJ*,

Dainotti M. G., Lenart A. L., Chraya A., Sarracino G., Nagataki S., Fraija N., Capozziello S., Bogdan M., 2022a, *MNRAS*,

Dainotti M. G., De Simone B. D., Schiavone T., Montani G., Rinaldi E., Lambiase G., Bogdan M., Ugale S., 2022c, *Galaxies*, **10**, 24

Dainotti M. G., De Simone B., Schiavone T., Montani G., Rinaldi E., Lambiase G., Bogdan M., Ugale S., 2022d, *Galaxies*, **10**, 24

Dainotti M. G., Sarracino G., Capozziello S., 2022e, *PASJ*, **74**, 1095

Dainotti M. G., et al., 2022f, *ApJS*, **261**, 25

Dainotti M. G., Nielson V., Sarracino G., Rinaldi E., Nagataki S., Capozziello S., Gnedin O. Y., Bargiacchi G., 2022g, *MNRAS*, **514**, 1828

Dainotti M. G., Bargiacchi G., Lenart A. L., Capozziello S., Ó Colgáin E., Solomon R., Stojkovic D., Sheikh-Jabbari M. M., 2022h, *ApJ*, **931**, 106

Dainotti M. G., Levine D., Fraija N., Warren D., Sourav S., 2022i, *ApJ*, **940**, 169

Dainotti M. G., Bargiacchi G., Bogdan M., Capozziello S., Nagataki S., 2023b, *JCAP* submitted

Dainotti M. G., Bargiacchi G., Lenart A., Nagataki S., Capozziello S., 2023a, *ApJ*

Dainotti M. G., Bargiacchi G., Bogdan M., Łukasz Lenart A., Iwasaki K., Capozziello S., Zhang B., Fraija N., 2023c, *arXiv e-prints*, p. [arXiv:2305.10030](https://arxiv.org/abs/2305.10030)

Dall'Osso S., Stratta G., Guetta D., Covino S., De Cesare G., Stella L., 2011, *A&A*, **526**, A121

Demianski M., Piedipalumbo E., Sawant D., Amati L., 2017, *A&A*, **598**, A113

Di Valentino E., Melchiorri A., Silk J., 2021, *Astrophys. J. Lett.*, **908**, L9

Efron B., Petrosian V., 1992, *ApJ*, **399**, 345

Efstathiou G., Gratton S., 2020, *Mon. Not. Roy. Astron. Soc.*, **496**, L91

Eisenstein D. J., et al., 2005, *ApJ*, **633**, 560

Escamilla-Rivera C., Capozziello S., 2019, *International Journal of Modern Physics D*, **28**, 1950154

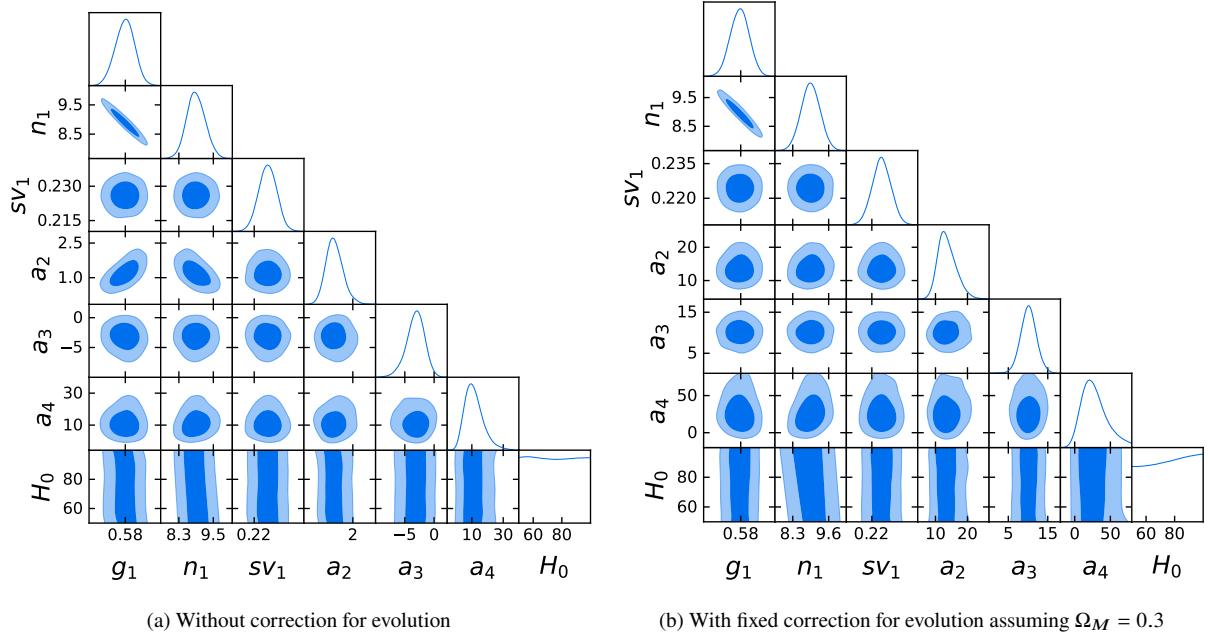


Figure 2. Fit of QSOs alone with \mathcal{L}_{new} for the evolutionary cases without correction for evolution (left panel) and with fixed correction for evolution assuming $\Omega_M = 0.3$ (right panel). For sake of visualization clarity, we do not show also the other two cases of fixed correction with $\Omega_M = 0.1$ and $\Omega_M = 0.9$ investigated in this work. These additional cases present similarities to the ones here shown and are described in detail in Table 1 and discussed in Sect. 4.1.

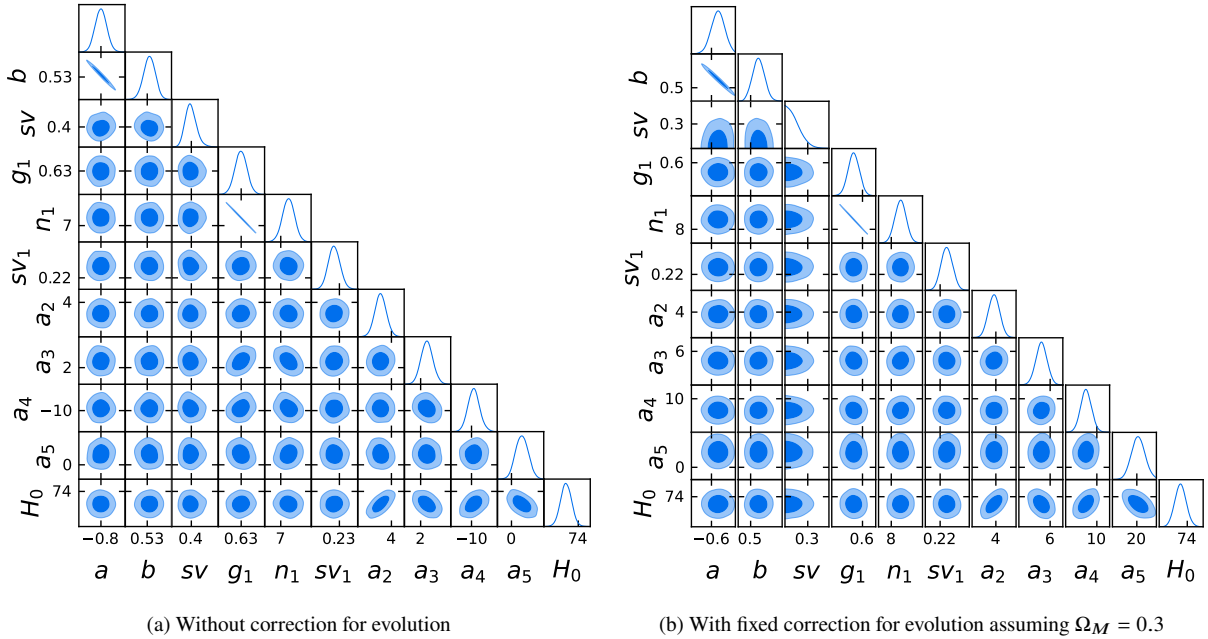


Figure 3. Fit of all probes together with $\mathcal{L}_{Gaussian}$ for the evolutionary cases without correction for evolution (left panel) and with fixed correction for evolution assuming $\Omega_M = 0.3$ (right panel). For sake of visualization clarity, we do not show also the other two cases of fixed correction with $\Omega_M = 0.1$ and $\Omega_M = 0.9$ investigated in this work. These additional cases present similarities to the ones here shown and are described in detail in Table 3 and discussed in Sect. 4.2.

Evans P. A., et al., 2009, *Monthly Notices of the Royal Astronomical Society*, **397**, 1177

Font-Ribera A., et al., 2014, *J. Cosmology Astropart. Phys.*, **2014**, 027

Freedman W. L., 2021, *ApJ*, **919**, 16

Gómez-Valent A., Amendola L., 2018, *J. Cosmology Astropart. Phys.*, **2018**, 051

Gonzalez J. E., Benetti M., von Martens R., Alcaniz J., 2021, *J. Cosmology*

Astropart. Phys., **2021**, 060

Hinshaw G., et al., 2013, *The Astrophysical Journal Supplement Series*, **208**, 19

Horowitz G. T., Teukolsky S. A., 1999, *Reviews of Modern Physics Supplement*, **71**, S180

Just D. W., Brandt W. N., Shemmer O., Steffen A. T., Schneider D. P., Chartas G., Garmire G. P., 2007, *ApJ*, **665**, 1004

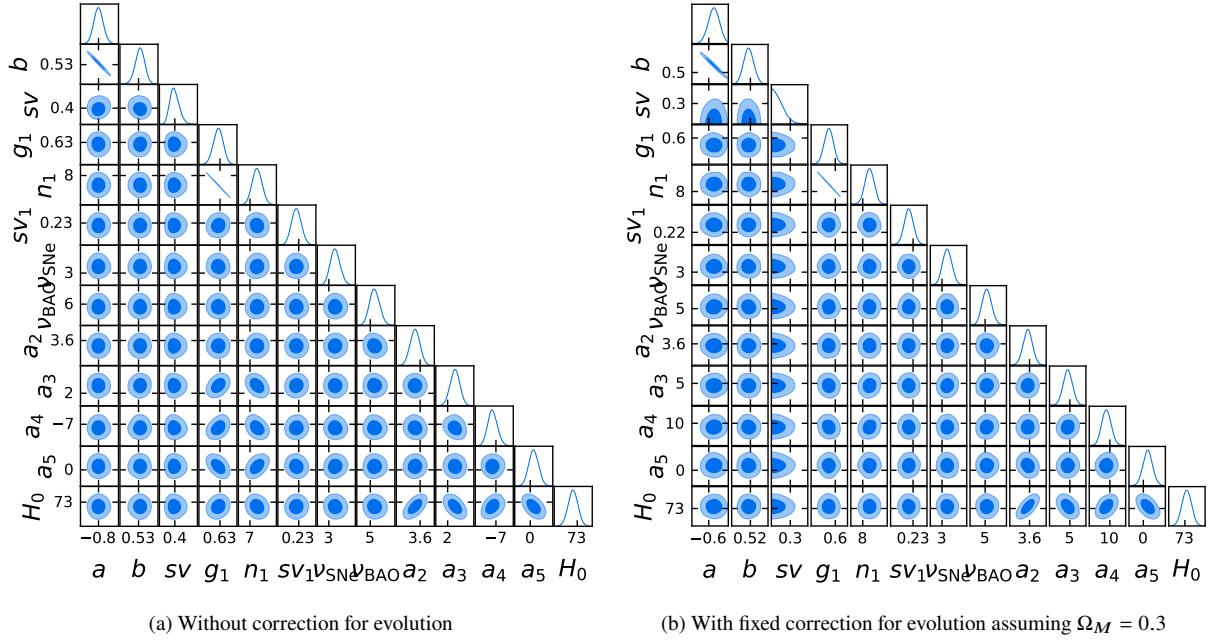


Figure 4. Fit of all probes together with \mathcal{L}_{new} for the evolutionary cases without correction for evolution (left panel) and with fixed correction for evolution assuming $\Omega_M = 0.3$ (right panel). For sake of visualization clarity, we do not show also the other two cases of fixed correction with $\Omega_M = 0.1$ and $\Omega_M = 0.9$ investigated in this work. These additional cases present similarities to the ones here shown and are described in detail in Table 3 and discussed in Sect. 4.2.

- Kelly B. C., 2007, *ApJ*, 665, 1489
- Khadka N., Ratra B., 2020a, *MNRAS*, 492, 4456
- Khadka N., Ratra B., 2020b, *MNRAS*, 497, 263
- Khadka N., Ratra B., 2021, *MNRAS*, 502, 6140
- Khadka N., Ratra B., 2022, *MNRAS*, 510, 2753
- Kocevski D., Liang E., 2006, *ApJ*, 642, 371
- Kroupa P., Subr L., Jerabkova T., Wang L., 2020, *MNRAS*, 498, 5652
- Lenart A. L., Bargiacchi G., Dainotti M. G., Nagataki S., Capozziello S., 2023, *ApJS*, 264, 46
- Levine D., Dainotti M., Zvonarek K. J., Fraija N., Warren D. C., Chandra P., Lloyd-Ronning N., 2022, *ApJ*, 925, 15
- Li Z., Huang L., Wang J., 2022, *MNRAS*, 517, 1901
- Liao K., Shafieloo A., Keeley R. E., Linder E. V., 2019, *ApJ*, 886, L23
- Lusso E., Risaliti G., 2016, *ApJ*, 819, 154
- Lusso E., et al., 2010, *A&A*, 512, A34
- Lusso E., Piedipalumbo E., Risaliti G., Paolillo M., Bisogni S., Nardini E., Amati L., 2019, *A&A*, 628, L4
- Lusso E., et al., 2020, *A&A*, 642, A150
- Netzer H., 2013, *Cambridge University Press*
- Peebles P. J., Ratra B., 2003, *Reviews of Modern Physics*, 75, 559
- Perlmutter S., et al., 1999, *ApJ*, 517, 565
- Petrosian V., Bouvier A., Ryde F., 2009, *arXiv e-prints*, p. arXiv:0909.5051
- Planck Collaboration et al., 2020, *A&A*, 641, A6
- Postnikov S., Dainotti M. G., Hernandez X., Capozziello S., 2014, *ApJ*, 783, 126
- Rea N., Gullón M., Pons J. A., Perna R., Dainotti M. G., Miralles J. A., Torres D. F., 2015, *ApJ*, 813, 92
- Rezaei M., Pour-Ojaghi S., Malekjani M., 2020, *ApJ*, 900, 70
- Riess A. G., et al., 1998, *AJ*, 116, 1009
- Riess A. G., et al., 2004, *ApJ*, 607, 665
- Riess A. G., et al., 2022, *ApJ*, 934, L7
- Risaliti G., Lusso E., 2015, *ApJ*, 815, 33
- Risaliti G., Lusso E., 2019, *Nature Astronomy*, p. 195
- Rodney S. A., et al., 2015, *AJ*, 150, 156
- Rowlinson A., Gompertz B. P., Dainotti M., O'Brien P. T., Wijers R. A. M. J., van der Horst A. J., 2014, *MNRAS*, 443, 1779
- Sahni V., Starobinsky A., 2000, *International Journal of Modern Physics D*, 9, 373
- Schiavone T., Montani G., Bombacigno F., 2022
- Scolnic D. M., et al., 2018, *ApJ*, 859, 101
- Scolnic D., et al., 2022, *ApJ*, 938, 113
- Sharov G. S., 2016, *J. Cosmology Astropart. Phys.*, 2016, 023
- Sharov G. S., Vasiliev V. O., 2018, *arXiv e-prints*, p. arXiv:1807.07323
- Singal J., Petrosian V., Lawrence A., Stawarz L., 2011, *ApJ*, 743, 104
- Srianand R., Gopal-Krishna 1998, *A&A*, 334, 39
- Srinivasaragavan G. P., Dainotti M. G., Fraija N., Hernandez X., Nagataki S., Lenart A., Bowden L., Wagner R., 2020, *The Astrophysical Journal*, 903, 18
- Steffen A. T., Strateva I., Brandt W. N., Alexander D. M., Koekemoer A. M., Lehmer B. D., Schneider D. P., Vignali C., 2006, *AJ*, 131, 2826
- Tananbaum H., et al., 1979, *ApJ*, 234, L9
- Tripp R., 1998, *A&A*, 331, 815
- Vagnozzi S., Loeb A., Moresco M., 2021, *ApJ*, 908, 84
- Visser M., 2004, *Classical and Quantum Gravity*, 21, 2603
- Wang F., et al., 2021, *ApJ*, 907, L1
- Wang B., Liu Y., Yuan Z., Liang N., Yu H., Wu P., 2022, *arXiv e-prints*, p. arXiv:2210.14432
- Weinberg S., 1972, *Gravitation and Cosmology: Principles and Applications of the General Theory of Relativity*
- Weinberg S., 1989, *Reviews of Modern Physics*, 61, 1
- Willingale R., et al., 2007, *ApJ*, 662, 1093
- Wong K. C., et al., 2020, *MNRAS*, 498, 1420
- Zamora Muñoz C., Escamilla-Rivera C., 2020, *J. Cosmology Astropart. Phys.*, 2020, 007
- Zamorani G., et al., 1981, *ApJ*, 245, 357
- Zhang B., Mészáros P., 2001, *ApJ*, 552, L35

This paper has been typeset from a $\text{\TeX}/\text{\LaTeX}$ file prepared by the author.